18TH WORLD CONFERENCE ON EARTHQUAKE ENGINEERING
WCEE2024
MILAN

MILAN, ITALY
30TH JUNE - 5TH JULY 2024

www.wcee2024.it

ENFRAG: ENHANCING STATE-DEPENDENT FRAGILITY THROUGH EXPERIMENTALLY VALIDATED ENERGY-BASED APPROACHES

R. Gentile[1], G. Angelucci[2], J. Wu[1], P. Morandi[3], R.R. Milanesi[3], F. Mollaioli[2], GJ. O'Reilly[4], F. Freddi[5], & F. Jalayer[1]

[1] Institute for Risk and Disaster Reduction, University College London, United Kingdom, r.gentile@ucl.ac.uk

[2] Department of Structural and Geotechnical Engineering, Sapienza University of Rome, Rome, Italy

[3] European Centre for Training and Research in Earthquake Engineering, Eucentre, Pavia, Italy

[4] Centre for Training and Research on Reduction of Seismic Risk (ROSE Centre), Scuola Universitaria Superiore IUSS Pavia, Italy

[5] Department of Civil, Environmental and Geomatic Engineering, University College London, United Kingdom

Abstract: *This paper presents the preliminary results of the ENFRAG research project, which is part of the ERIES project (engineering research infrastructures for European synergies). ENFRAG aims at advancing state-dependent earthquake fragility assessment methodologies. The project involves sequential quasi-static cyclic displacement-controlled in-plane (IP) and shaking-table dynamic out-of-plane (OOP) tests on four nominally identical infill walls. Different load protocols are employed to induce the same peak-based engineering demand parameters (EDPs) while modulating the energy-based demands. A multi-fidelity approach is employed to integrate the experimental data with synthetic datasets including IP cloud-based analysis, IP quasi-static, push-pull analyses with different load protocols, OOP dynamic analyses, and IP-OOP combined analyses. The results are used to explore the potential of energy-based EDPs for interpreting damage states and damage accumulation. This allows experimentally validating methodologies to derive state-dependent fragility functions that account for multiple sources/mechanisms of damage accumulation. This contribution provides an update on the numerical and analytical components of ENFRAG, as well as linking them with the specific research objectives.*

1 Introduction

Fragility functions play a crucial role in seismic risk assessment, allowing for the prioritisation of retrofitting efforts, the development of more effective building codes, and the allocation of resources for disaster preparedness and response. Fragility functions describe the probability of different assets reaching or exceeding different damage states (DSs) conditioned on an earthquake intensity measures (IMs). DSs are usually represented by thresholds of engineering demand parameters (EDPs) often represented by peak deformation quantities such as displacements, drifts or accelerations (i.e., ground or floor). Monotonic or quasi-static cyclic testing can conveniently provide such deformation thresholds for a given structural system or component, thus providing proxies of the peak structural demand under different ground motions. This is ideal from an economic point of view since such tests do not depend on a specific ground-motion excitation input (thus not requiring several tests).

Recent research (Di Trapani and Malavisi, 2019; Papadopoulos et al., 2020) has investigated damage state-dependent fragility relationships useful for structures subjected to ground motion sequences (e.g., mainshock-aftershock). Most studies use the peak inter-storey drift as the measure of damage, although some models also take residual drift into account (Zhang et al., 2020). Peak or residual quantities, however, cannot properly capture damage accumulation since they do not monotonically increase with ground-motion intensity. Moreover, using these EDPs for state-dependent fragility analysis can lead to statistical inconsistencies. For example, a structure subjected to a given peak deformation (e.g., drift) will sustain a certain level of damage. If the structure is subsequently subjected to the same deformation level, the actual damage level is likely to increase. If damage is measured with peak deformation-based DS thresholds, the structure will not be assigned a higher DS, which is inconsistent.

Integral quantities, such as hysteretic energy (E_h), can solve the above inconsistency since they monotonically increase with the ground-motion excitation (or sequence) length. A recent study by Gentile and Galasso (2021) provides a hysteretic energy-based framework for state-dependent fragility. The framework takes advantage of the demonstrated pseudo-parabolic relationship between the peak global deformation (e.g., maximum inter-storey drift) and the hysteretic energy of a system (Figure 1). By characterising the median of this relationship via numerical analyses, it is possible to convert deformation-based damage thresholds into energy-based ones and characterise state-dependent fragility functions. The authors highlight that even though the framework is theoretically sound, an experimental validation is needed.

The ERIES-ENFRAG project (ENhancing state-dependent FRAGility through experimentally validated Energy-Based Approaches), led by University College London, sheds some light on the above research gap. ERIES-ENFRAG explores the experimental validation of hysteretic energy-based fragility assessment approaches, which are: 1) Currently based only on analytical and/or numerical validations; 2) Only considering one type of action/damage mechanism. The project focuses on masonry infill walls experiencing cumulative states of damage due to combinations of in-plane (IP) and out-of-plane (OOP) actions, commonly quantified through two different peak-based engineering demand parameters (EDPs). Extensive analytical and numerical studies are adopted to define specific loading protocols adopted for this study. This allows the experimental results to be used in a multi-fidelity statistical approach -combining experimental and numerical data- and to maximise the statistical power of the inferences drawn from the results.

Apart from this introduction, the paper is structured as follows: Section 2 provides some details about the experimental campaign and the related numerical studies for its calibration and interpretation; Section 3 describes the preliminary results available at the time of submitting this manuscript.

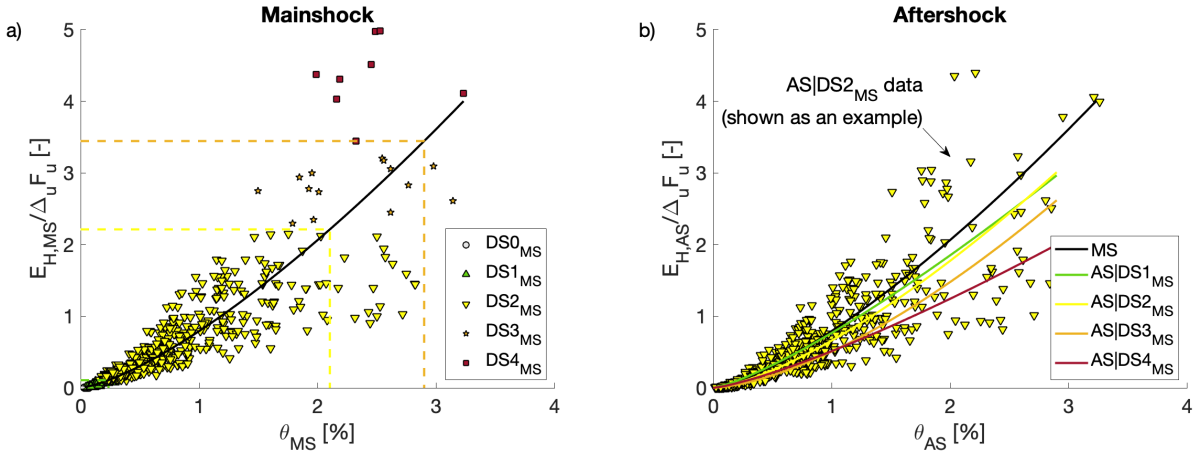

Figure 1. Hysteretic energy vs maximum inter-storey drift relationship for a case-study RC frame: a) mainshock; b) aftershock (dependent on the damage state in the mainshock). Gentile & Galasso, 2021)

2 Methodology

The core of the ERIES-ENFRAG project is an experimental campaign involving sequential quasi-static cyclic displacement-controlled IP and shaking-table dynamic OOP tests for four nominally identical masonry infill

walls (Figure 2) which are described in Section 2.1. These are tested with different load protocols with the goal of inducing the same values of peak-based EDPs while modulating the energy-based demand conditional to the above peak EDPs. The overall goal is the effective characterisation of the $E_h|EDP_{IP}$ and $E_h|EDP_{OOP}$ relationships, which are strongly dependent on the input load excitation. Analysing only four load protocols may not allow robust inferences on the above relationships to be obtained. To compensate this, numerical analyses involving macro- and micro-modelling approaches (Section 2.2) are used to produce an intelligently-defined design of experiment of loading protocol. This process exploits the results of an experimental campaign (Kurukulasuriya et al., 2023) conducted in the same laboratory, with the same setup, and specimens nominally identical to the ones adopted herein. Moreover, a synthetic design of the experiment is first carried out and comprises multiple runs of a macro model calibrated using the experimental data. Section 2.3 describes this process, as well as how micro-modelling aids the interpretation of the results (with particular reference to the definition of damage states).

2.1 Experimental campaign

Cyclic quasi-static and shaking-table tests on masonry infills both IP and OOP are performed using a surrounding frame (Figure 2a). In real settings and in available literature, this is typically made of reinforced concrete or steel. For economical and time-saving reasons, in a previous experimental campaign (Kurukulasuriya et al., 2023) a composite frame is used to encase the infill panels. In the present study, the same frame will be adopted to also allow direct comparisons with past and ongoing experimental studies. The frame is designed to remain elastic and to mimic the stiffness of typical concrete frame members built in the Mediterranean area between the 1960s and 1980s, with no seismic provisions. The considered masonry infills (Figure 2b) are 3.5m long, 2.75m high, and 13cm thick, with 10mm of plaster on one side. The masonry is made of hollow clay units with general purpose mortar in the joints. Moreover, the head-joints have been poorly made to replicate the construction practise of the time. The panels are in full adherence with the structural frame .

(a) (b)

Figure 2. (a) Structural frame; (b) masonry infill at the end of the construction (Kurukulasuriya et al., 2023).

Two different experimental setup configurations are considered for IP and OOP tests (Figure 3). In the IP phase, a specimen is fixed to the shaking table (used as a stable floor) to keep the foundation beam and the shaking table from moving relative to each other. The displacement-controlled pseudo-static cyclic IP tests will be regulated by a hydraulic actuator connected to an external rigid steel structure. Additionally, four inclined bracing systems are employed to stop any OOP motion of the surrounding frame. The IP test is monitored through linear transducers. For the OOP tests, the hydraulic actuator is detached, but the OOP restraints are still attached to the specimen, and the ground motion excitation is applied through the shaking table. The dynamic tests are monitored through accelerometers and an external 3D displacement acquisition system. The response of the masonry panel is also monitored through a pattern of instruments located in different areas.

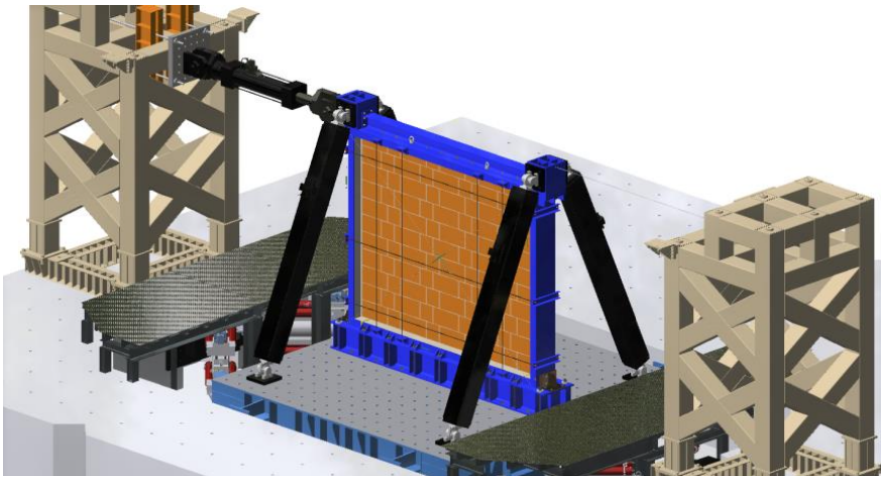

Figure 3. Sketch of the experimental setup adopted for the quasi-static IP and dynamic OOP tests (Kurukulasuriya et al., 2023).

The four nominally-identical specimens are subjected to a test sequence of a quasi-static, cyclic IP phase, followed by shaking-table dynamic OOP loading. The IP phase consists of a displacement-controlled loading imposing d levels of horizontal drift $\theta_{max} = [\theta_1, \dots, \theta_d]$, each involving full cycles $[0, \theta_{max}, -\theta_{max}, 0]$ repeated c times. Starting from the IP-damaged configuration, the OOP phase then consists of a series of dynamic shaking-table runs where the same seismic excitation ($a(t)_{OOP}$) is applied with increased intensity at regular intervals up to the OOP collapse of the specimen. Since the applied excitation is interpreted as a floor acceleration, the peak floor acceleration is used as the OOP intensity measure, and the different runs are regulated by its increment (ΔPFA_{OOP}).

The experimental campaign is designed by modulating the parameters θ_{max} (and consequently, d), c, $a(t)_{OOP}$, and ΔPFA_{OOP} to subject the specimens to the same values of peak-based EDPs while modulating the energy-based demand conditional to the above peak quantities ($E_h|EDP_{IP}$ and $E_h|EDP_{OOP}$), as shown in Table 1. Moreover, this project exploits four reference specimens (Ref1-4) tested by Kurukulasuriya et al. (2023) under a regime similar to the one proposed in ERIES-ENFRAG. In particular, the baseline specimen (Ref1) involves an IP phase with $d = 7$ drift levels nominally up to 0.65% ($c = 3$ cycles per level). The OOP phase for this specimen was conducted using an excitation compliant with the required response spectrum method within AC156, and $\Delta PFA_{OOP} = 0.1g$ intervals of peak floor acceleration. Ref 2-4 in Kurukulasuriya et al., (2023) investigated the influence of the maximum IP drift on the OOP performance, together with the pure IP capacity. Although such data is used for the numerical investigations, this parameter is not explicitly investigated in the proposed test campaign.

Table 1 shows a draft of the loading protocols for the campaign. Such values are subjected to refinements based on the extensive analytical and numerical calibration study described in Section 2.3, which is still ongoing. Tests 1-4, are defined starting from specimen Ref 1 and changing only one of the above-mentioned loading parameters (Table 1). This results in having: a specimen with higher-than-baseline IP hysteretic energy, having $c = 5$ cycles per drift level (Test 1); a specimen with lower-than-baseline IP hysteretic energy, having $d = 3$ drift levels (Test 2); a specimen with higher-than-baseline OOP hysteretic energy having $\Delta PFA_{OOP} = 0.05g$ peak floor acceleration increment (Test 3); a specimen with lower-than-baseline OOP hysteretic energy, having an excitation with half the significant duration than the standard AC156 (Test 4).

Table 1. Draft of the test programme

Test	θ_{max}	d	c	$a(t)_{OOP}$	ΔPFA_{OOP}	Notes
Ref1*	[0.05, 0.1, 0.2, 0.3, 0.4, 0.5, 0.65]%	**7**	**3**	**AC156**	**0.10g**	**Baseline**; severe IP damage
Ref2*	[0.05, 0.1, 0.2, 0.3]%	4	3	AC156	0.10g	Reference; moderate IP damage
Ref3*	No IP test	-	-	AC156	0.10g	Reference; only OOP to measure capacity
Ref4*	[0.05, 0.1, 0.2, 0.3, 0.4, 0.5, 0.75, 1]%	7	3	-	-	Reference; only IP to measure capacity
Test1	[0.05, 0.1, 0.2, 0.3, 0.4, 0.5, 0.65]%	7	**5**	AC156	0.10g	**more** $E_h\|EDP_{IP}$ increasing EDP_{IP} cycles
Test2	[0.05, 0.3, 0.65]%	**3**	3	AC156	0.10g	**less** $E_h\|EDP_{IP}$ decreasing EDP_{IP} levels
Test3	[0.05, 0.1, 0.2, 0.3, 0.4, 0.5, 0.65]%	7	3	AC156	**0.05g**	**more** $E_h\|EDP_{OOP}$ with more PFA levels
Test4	[0.05, 0.1, 0.2, 0.3, 0.4, 0.5, 0.65]%	7	3	**AC156 half duration**	0.10g	**less** $E_h\|EDP_{OOP}$ changing frequency content of PFA input

d: target IP drift levels; θ_{max}: maximum drift at each target; c: number of cycles per target drift; ΔPFA_{OOP}: PFA increment up to collapse; *: results from Kurukulasuriya et al., (2023).

2.2 Numerical Modelling Strategies

Two modelling strategies are considered here to numerically simulate the IP and OOP response of infilled specimens, namely the macro- and micro-modelling approaches. In the former case (Figure 4a), the infill response under in-plane horizontal loads is reproduced by adopting an equivalent strut macro-model and by using the "HystereticSM" uniaxial material in OpenSees (McKenna et al., 2007). The infill panel is modelled by two concentric compression-only diagonal struts and a multi-linear envelope is implemented for the force-deformation relationship according to the constitutive model proposed by Liberatore et al. (2018). Specifically, the peak strength of the backbone curve is computed by considering different failure mechanisms according to Decanini and Fantin (1986). For the IP cyclic response of the infill, the hysteretic parameters for stiffness and strength degradation are calibrated based on available experimental data (see Section 2.3).

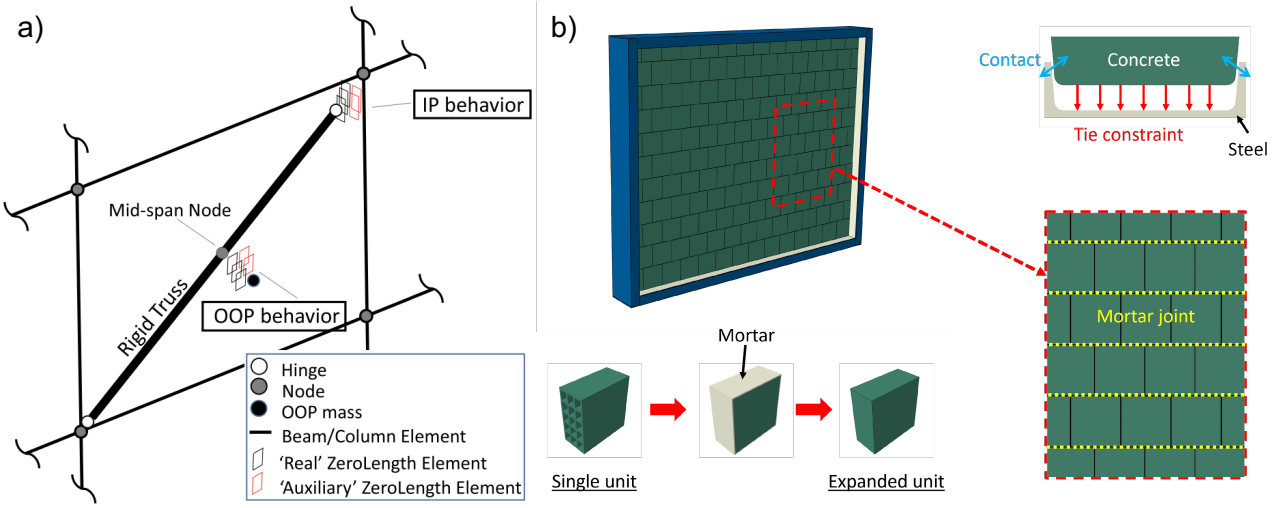

Figure 4. Numerical modelling strategies: a) macro modelling (modified after Ricci et al., 2018*); b) micro modelling.*

On the other hand, the modelling strategy adopted for both the OOP response of the infills and the IP-OOP interaction effects follows the approach proposed by Ricci et al. (2018). To reflect the OOP behaviour of the infill, a central node with lumped OOP mass is pin-connected to the surrounding frame via a semi-diagonal nonlinear link, which is provided with a single degree of freedom and a trilinear force-displacement relationship ("Hysteretic uniaxial" material in OpenSees). The mutual IP-OOP interaction is numerically simulated by altering the OOP backbone parameters as a function of the recorded IP damage. Therefore, the OOP strength and stiffness degradation are triggered once a certain IP displacement demand is attained.

Finite element micro models of the specimens (Figure 4b) are also established in Abaqus (Dassault Systèmes, 2014) adopting the micro-modelling approach (Abdulla et al., 2017). All the model components (i.e., the steel beams and columns, the concrete part, the bricks, and the plaster) are modelled using solid elements ("C3D8R"). The bare frame is designed to remain elastic during the tests, and therefore only the elastic behaviour is defined for the C-shaped steel members and the filling concrete. While the elastic moduli of steel and concrete in the frame are initially assumed to be 210GPa and 35GPa, respectively, they are then reduced to match the initial stiffness of the bare frame measured during the tests in Kurukulasuriya et al., (2023). Tie constraints are employed between the steel member and the related concrete fillings to simulate the effects of shear studs according to the real detailing of the specimens, as illustrated in Figure 4b. Moreover, contacts are defined between the concrete part and the flanges of the steel members, considering 'Hard' normal behaviour and a friction coefficient equal to 0.3. The modelling of the infill wall comprises "expanded brick units", which comprise the brick units and the surrounding mortar. This allows for simplification of the micro-modelling strategy by omitting the mortar layers and simulating the mortar joints through appropriate surface-based contact definitions. Moreover, a layer of plaster is also considered on one side of the wall. The elastic and inelastic properties of the brick units, the latter simulated by the built-in Concrete Damage Plasticity (CDP) material model, are defined based on the compressive tests of wallets available from the tests in Kurukulasuriya et al., (2023). Similarly, the inelastic properties of the plaster layer are also modelled by the CDP model, considering the measured compressive and tensile strength of mortar.

Furthermore, the mortar joint was modelled by employing the surface-to-surface contact approach, whose behaviour is described by the traction-separation law in Abaqus (Dassault Systèmes, 2014). The damage initiation is defined considering a quadratic stress criterion depending on both normal and shear stresses. In particular, the critical shear stress of the mortar joint is described by a Mohr–Coulomb failure criterion, where the cohesion and the friction coefficient are determined from triplet tests. Additionally, damage evolution is described by the Benzeggagh-Kenane law (Benzeggagh and Kenane, 1996), which determines the critical mixed-mode fracture energy which follows an exponential function of the slip. Additional details about the modelling strategy are described in Wu et al. 2022.

2.3 Synthetic Dataset and Interaction with the Experimental Campaign

This section describes how several types of numerical analyses are used to enhance the experimental dataset aiming at increasing the robustness of the statistical inferences of ERIES-ENFRAG. For brevity, the description herein involves the IP behaviour only, although an analogous procedure is conducted for the OOP behaviour.

First, the monotonic behaviour of the specimen is calibrated based on mechanics-based relationships. For the macro-model, the stiffness of the (elastic) surrounding frame is obtained by matching it with the experimental results in Kurukulasuriya et al. (2023). The backbone force-displacement curve of the infill (macro model) is computed consistently to the model by Decanini and Fantin (1986). In parallel, a micro model is also calibrated according to Section 2.2. Pushover analyses are conducted for both models and the results are compared to the available experimental data, which initially refers to the experimental campaign in Kurukulasuriya et al. (2023). This allows for a first sanity check of the models, including minor refinements in the mechanics-based calibrations.

The hysteretic parameters of the macro model are calibrated are calibrated using a maximum likelihood estimator and making use of all the available experimental data. This is done using the quasi-static, cyclic IP data related to the specimens Ref 1, Ref 2, and Ref 4 expressed in the form ${E_H}^{EXP,k}(\theta_{max,i})$. In this notation, k indicates the specimen and its IP load protocol (see Table 1), while $\theta_{max,i}$ indicates the absolute value of the maximum drift experienced by the specimen up to step i of the test (note that the test is monitored several times per each drift cycle). A macro model is developed as a function of the vector of the parameters of the "HystereticSM" model in OpenSees, $H = [h_1, \dots, h_5]$, and the push-pull load protocol, $load_k$, consistent with the considered experimental tests. The hysteretic energy calculated for such analyses is ${E_H}^{NUM,k}(\theta_{max,i}, H)$, where the superscript k indicates the load protocol.

Consistently with Gardoni et al. (2002), the likelihood of the macro model to observe the test data ${E_H}^{EXP,k}(\theta_{max,i})$ is expressed by Eq. 1. In such equation, σ is a parameter expressing model uncertainty, ${r_i}^k(H)$ represents a distance function between the experimental and numerical hysteretic energy (Eq. 2), and φ is the standard Normal probability density function. Through a non-linear optimiser, Eq. 1 is maximised to find the

optimal vector of hysteretic parameters H^*. Depending on the available computational power, an analogous approach may be performed for the micro model of the specimen.

$$L(H,\sigma) \propto \prod_{i,k} \frac{1}{\sigma\theta_{max,i}} \varphi\left[\frac{r_i^k(H)}{\sigma\theta_{max,i}}\right] \quad (1)$$

$$r_i^k(H) = \left|{E_H}^{EXP,k}(\theta_{max,i}) - {E_H}^{NUM,k}(\theta_{max,i}, H)\right| \quad (2)$$

A cloud analysis is carried out for the optimised model adopting a large set of unscaled real (i.e., recorded) ground motions. The results are used to characterise the probability distribution of the dynamic hysteretic energy vs maximum deformation (i.e., $E_h|\theta_{max}$), consistently with the format in Figure 1a. In parallel, a parametric push-pull analysis of the optimised model is conducted by varying the cyclic load parameters (i.e., c, d). This allows providing the mapping (c, d) vs $E_h(\theta_{max})$. The above mapping is adopted to refine the parameters (c, d) used for Tests 1-4 of the experimental campaign (Table 1), ensuring an adequate match of specific percentiles of the dynamically-derived $E_h|\theta_{max}$ distribution.

After running the experimental campaign, the optimised numerical models (both macro and micro models) are adopted to reproduce the experimental campaign. On the one hand, this allows a more detailed interpretation of the damage patterns measured in the tests. On the other hand, a combined experimental and synthetic dataset is created to allow statistically testing the hypotheses connected with ERIES-ENFRAG (detailed in Section 4) in a multi-fidelity approach.

Finally, it is worth mentioning that an analogous procedure is conducted for the OOP behaviour. In this case: IP push-pull analyses are substituted with OOP incremental dynamic analyses; IP cloud analyses are substituted with OOP dynamic analyses reproducing the loading history generated in the laboratory experiment (i.e., a “sequential incremental dynamic analysis”). When relevant, IP analyses are combined with the OOP behaviour to simulate the state-dependent behaviour.

3 Preliminary Results

At the time of writing this paper, the experimental tests named “Test 1-4” (Table 1) have not been conducted yet, and the investigation is focused on the preliminary numerical studies for the refinement of the load protocols to adopt. The available numerical results refer to the preliminary calibration of the numerical models and their verification against the available experimental data. Within this section, the data related to the IP loading of Ref 4 (Table 1) is adopted. Figure 5a shows the related force-displacement curves considering: the elastic response of the frame; the quasi-static, cyclic response of the entire specimen; the envelope of such cyclic response; and the infill-only envelope.

The monotonic behaviour of the specimen is macro-modelled using a mechanics-based constitutive law (i.e., not adopting manual adjusting to match the experimental results). To appreciate the predictive capabilities of the selected equivalent strut strategy, the response of the infill panel is considered in isolation. As an example, a comparison of the numerical backbone and the experimental envelope is illustrated in Figure 5b. The defined numerical model satisfactorily predicts the elastic phase up to the first cracking of the infill: both the stiffness and strength provide a good match with the experimental results. The post-cracking envelope up to peak strength is slightly different depending on the considered load direction. The positive peak load is equal to 135.7kN (163.2kN for the numerical model) while it is equal to 162.1kN for the negative side (162.7kN for the numerical model). The post-peak strength deterioration of the infill backbone shows major discrepancies with the experimental data. Most likely, this is due to the great uncertainty on the ultimate displacement prediction of the model by Liberatore et al. (2018), which likely yields to poor predictions of the softening branch. Overall, the numerical backbone shows a satisfactory agreement with the envelope of the experimental test, and it is therefore deemed suitable for this research.

As a further validation, the micro model is also adopted. Initially, this model is subjected to cyclic loadings at small displacement amplitudes to simulate the complete cracking between the wall and the confining frame. Subsequently, due to the considerable computational demand, the lateral (top) displacement of the model is increased monotonically. The force-displacement response predicted by the micro-model is also included in Figure 5b, which is in good agreement with both the experimental envelope and the backbone of the macro

model. Two damage states are defined consistently with the interpretation of the experimental campaign by Kurukulasuriya et al. (2023): Operation Limit State (OLS) and Damage Limit State (DLS). They are also indicated in Figure 5b. Somehow consistently with the macro model, the micro model provides a very good approximation of the experimental force-displacement response up to OLS. For larger displacements, especially after DLS, the discrepancy increases, and the micro model does not accurately capture the softening behaviour. Despite this limitation, the micro model provides a close estimation of the crack pattern compared to the real damage observed during the tests, as highlighted in Figure 5c, which also shows the stress distribution at DLS. Evidently, the infill wall exhibited a single diagonal-strut mechanism prior to the occurrence of the first major diagonal crack, which then turned into a multiple-strut mechanism.

The above results allow validating the numerical estimation of the backbone, which is considered deterministic in the following. To calibrate the hysteretic parameters of the macro model, the hysteretic energy vs peak displacement curves of the experimental tests are first derived, and Equations 1 and 2 are encapsulated in a nonlinear optimiser. At each iteration, a set of hysteresis parameters is sampled, push-pull analyses are run consistently with the available experimental data (Ref 1, 2, 4), and the likelihood is computed. The resulting push-pull response of the maximum-likelihood model is shown in Figure 5d, highlighting a close match between the experimental and numerical data.

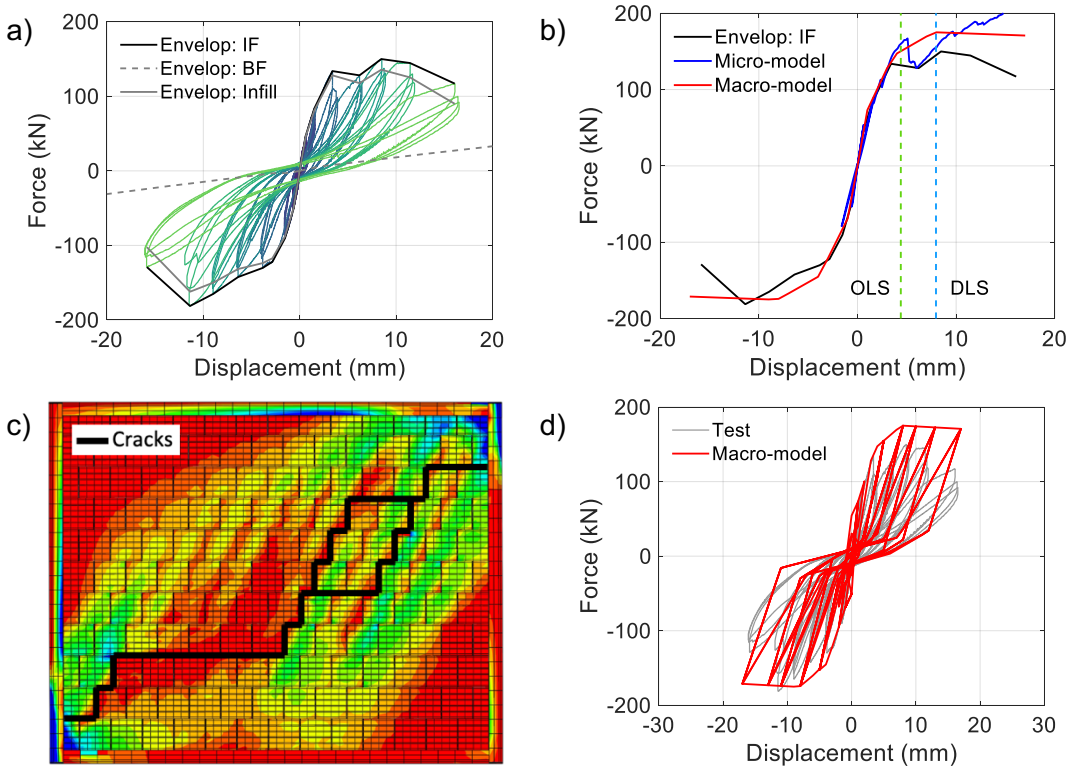

Figure 5. a) Experimental data for the Ref 4 test (Data from Kurukulasuriya et al., 2023); *b) Comparisons of the experimental and numerical results of the force-displacement response of the infilled frame; c) Push-pull analysis of the optimised macro model compared to the experimental measurements; d) Predicted distribution of minimum principal stress and deformation of the infilled frame at the damage limit state (SLD)*

4 Final Remarks

The ERIES-ENFRAG research project aims at advancing state-dependent earthquake fragility assessment methodologies. The project involves sequential quasi-static cyclic displacement-controlled in-plane (IP) and shaking-table dynamic out-of-plane (OOP) tests on four nominally identical infill walls. Different load protocols are employed to induce the same peak-based engineering demand parameters (EDPs) while modulating the energy-based demands. A multi-fidelity approach is employed to integrate the experimental data with synthetic datasets including IP cloud-based analysis, IP quasi-static, push-pull analyses with different load protocols, OOP dynamic analyses, and IP-OOP combined analyses. The results are used to explore the potential of energy-based EDPs for interpreting damage states and damage accumulation. This allows experimentally

validated methodologies to derive state-dependent fragility functions that account for multiple sources/mechanisms of damage accumulation. This contribution provides an update on the numerical and analytical components of ENFRAG, as well as linking them with the specific research objectives.

At the time of writing, the experimental campaign has not been conducted yet. However, the objectives of the research are:

1. To study the influence of the shape (i.e., number of cycles and relative amplitude) of the IP quasi-static cyclic loading protocol on the hysteretic energy vs. drift relationship of masonry infill walls and its relation to the dynamic evaluation (numerical) of the same relationship;
2. To provide a methodology to characterise the (dynamic) median hysteretic energy vs. drift relationship of masonry infill walls based on a quasi-static cyclic test;
3. To develop a methodology to "correct" fragility functions (i.e., discount the often-overlooked cumulative damage) of masonry infills empirically derived from shaking-table tests. A related objective is to render the procedure extendable to other structures/structural components;
4. To investigate the influence of the OOP dynamic loading protocol on the hysteretic energy vs. peak acceleration relationship of masonry infill walls;
5. To provide valuable experimental data and harmonise the IP and OOP damage characterisation under the same energy-based methodology, thus advancing the study of the influence of IP damage on the OOP dynamic behaviour of masonry infills, which is still an unresolved topic.

Although, the project focuses on masonry infill walls, it has the potential of paving the way for similar cumulative-damage tests for different structures/structural components through the overall approach adopted whilst also providing experimental data on masonry infills' IP and OOP response. ERIES-ENFRAG aims at a robust consideration of damage accumulation, particularly relevant in mainshock-aftershock conditions, and will also shed further light on the appropriateness of IP and OOP cyclic loading protocols used in experimental testing.

Acknowledgements

This work is part of the transnational access project "ERIES–ENFRAG", supported by the Engineering Research Infrastructures for European Synergies (ERIES) project (www.eries.eu), which has received funding from the European Union's Horizon Europe Framework Programme under Grant Agreement No. 101058684. This is ERIES publication number C2.

References

Abdulla, K.F., Cunningham, L.S., Gillie, M., 2017. Simulating masonry wall behaviour using a simplified micro-model approach. Eng Struct 151, 349–365. https://doi.org/10.1016/j.engstruct.2017.08.021

Benzeggagh, M.L., Kenane, M., 1996. Measurement of mixed-mode delamination fracture toughness of unidirectional glass/epoxy composites with mixed-mode bending apparatus. Compos Sci Technol 56, 439–449. https://doi.org/10.1016/0266-3538(96)00005-X

Dassault Systèmes, 2014. ABAQUS/Standard User's Guide, Version 6.14. . Providence.

Decanini, L., Fantin, G., 1986. Modelos simplificados de la mampostería incluida en porticos. Caracteristicas de stiffnessy resistencia lateral en estado limite, in: Jornadas Argentinas de Ingeniería Estructural. pp. 817–836.

Di Trapani, F., Malavisi, M., 2019. Seismic fragility assessment of infilled frames subject to mainshock/aftershock sequences using a double incremental dynamic analysis approach. Bulletin of Earthquake Engineering 17, 211–235. https://doi.org/10.1007/s10518-018-0445-2

Gardoni, P., Der Kiureghian, A., Mosalam, K.M., 2002. Probabilistic Capacity Models and Fragility Estimates for Reinforced Concrete Columns based on Experimental Observations. J Eng Mech 128, 1024–1038. https://doi.org/10.1061/(ASCE)0733-9399(2002)128:10(1024)

Gentile, R., Galasso, C., 2021. Hysteretic energy-based state-dependent fragility for ground-motion sequences. Earthq Eng Struct Dyn 50, 1187–1203. https://doi.org/10.1002/eqe.3387

Kurukulasuriya, M., Milanesi, R.R., Magenes, G., Bolognini, D., Grottoli, L., Dacarro, F., Morandi, P., 2023. Investigation of seismic behaviour of existing masonry infills through combined cyclic in-plane and dynamic out-of-plane tests, in: COMPDYN 2023 9th ECCOMAS Thematic Conference on Computational Methods in Structural Dynamics and Earthquake Engineering.

Liberatore, D., Addessi, D., Sangirardi, M., 2018. On the degrading/hysteretic response of masonry under seismic loads, in: 10th International Masonry Conference, IMC 2018. Milano.

McKenna, F., Fenves, G., Scott, M., 2007. OpenSees: open system for earthquake engineering simulation, Pacific Earthquake Engineering Research Center.

Papadopoulos, A.N., Kohrangi, M., Bazzurro, P., 2020. Mainshock-consistent ground motion record selection for aftershock sequences. Earthq Eng Struct Dyn. https://doi.org/10.1002/eqe.3263

Ricci, P., Di Domenico, M., Verderame, G.M., 2018. Empirical-based out-of-plane URM infill wall model accounting for the interaction with in-plane demand. Earthq Eng Struct Dyn 47, 802–827. https://doi.org/10.1002/eqe.2992

Wu, J.R., Di Sarno, L., Freddi, F., D'Aniello, M (2022). Modelling of Masonry Infills in Existing Steel Moment-Resisting Frames: Nonlinear Force-Displacement Behaviour. Engineering Structures, 267: 114699. https://doi.org/10.1016/j.engstruct.2022.114699

Zhang, L., Goda, K., De Luca, F., De Risi, R., 2020. Mainshock-aftershock state-dependent fragility curves: A case of wood-frame houses in British Columbia, Canada. Earthq Eng Struct Dyn 1–20. https://doi.org/10.1002/eqe.3269